EARTHQUAKE ENGINEERING AND STRUCTURAL DYNAMICS
*Earthquake Engng Struct. Dyn.* 2007; **36**:1973–1997
Published online 15 June 2007 in Wiley InterScience (www.interscience.wiley.com). DOI: 10.1002/eqe.694

# Evaluation of the seismic performance of a code-conforming reinforced-concrete frame building—from seismic hazard to collapse safety and economic losses

Christine A. Goulet[1,*,†], Curt B. Haselton[2], Judith Mitrani-Reiser[3], James L. Beck[3], Gregory G. Deierlein[2], Keith A. Porter[3] and Jonathan P. Stewart[1]

[1]*Department of Civil and Environmental Engineering, UCLA, Los Angeles, CA 90095, U.S.A.*
[2]*Department of Civil and Environmental Engineering, Stanford University, Stanford, CA 94305, U.S.A.*
[3]*Division of Engineering and Applied Science, Caltech, Pasadena, CA 91125, U.S.A.*

## SUMMARY

A state-of-the-art seismic performance assessment is illustrated through application to a reinforced-concrete moment-frame building designed per current (2003) building code provisions. Performance is quantified in terms of economic losses and collapse safety. The assessment includes site-specific seismic hazard analyses, nonlinear dynamic structural response simulations to collapse, damage analyses, and loss estimation. When selecting ground motion records for nonlinear dynamic analyses that are consistent with a target hazard level expressed in terms of a response spectral value at the building's fundamental period, it is important to consider the response spectral shape, especially when considering higher hazard levels. This was done through the parameter commonly denoted by $\varepsilon$. Neglecting these effects during record selection is shown to lead to a factor of 5–10 overestimation of mean annual collapse rate. Structural response simulations, which properly account for uncertainties in ground motions and structural modelling, indicate a 2–7% probability of collapse for buildings subjected to motions scaled to a hazard level equivalent to a 2% probability of exceedance in 50 years. The probabilities of component damage and the means and coefficients of variation of the repair costs are calculated using fragility functions and repair-cost probability distributions. The calculated expected annual losses for various building design variants range from 0.6 to 1.1% of the replacement value, where the smaller losses are for above-code design variants and the larger losses are for buildings designed with minimum-code compliance. Sensitivity studies highlight the impact of key modelling assumptions on the accurate calculation of damage and the associated repair costs. Copyright © 2007 John Wiley & Sons, Ltd.

Received 31 August 2006; Revised 31 January 2007; Accepted 22 March 2007

KEY WORDS: seismic; performance; assessment; building; epsilon; collapse; losses

*Correspondence to: Christine A. Goulet, Department of Civil and Environmental Engineering, UCLA, Los Angeles, CA 90095, U.S.A.
†E-mail: christinegoulet@engineering.ucla.edu

Contract/grant sponsor: Earthquake Engineering Research Centers Program of the National Science Foundation; contract/grant number: EEC-9701568
Contract/grant sponsor: National Sciences and Engineering Research Council of Canada
Contract/grant sponsor: le Fonds québécois de la recherche sur la nature et les technologies

## 1. INTRODUCTION

Performance-based earthquake engineering (PBEE) consists of the evaluation, design and construction of structures to meet seismic performance objectives that are meaningful for the structures' stakeholders (expressed in terms of dollars, deaths, or downtime). Figure 1 illustrates the PBEE methodology developed by the Pacific Earthquake Engineering Research (PEER) Center [1]. This methodology involves combined numerical integration of all the conditional probabilities in Figure 1 to propagate the uncertainties from one level of analysis to the next, resulting in probabilistic prediction of performance. The first step in PBEE is the hazard analysis, in which the mean annual rate of exceedance of a particular ground-shaking intensity measure IM (or a vector of IMs) is evaluated for the site considering local seismic sources and their characteristics. We take the spectral acceleration at the fundamental-mode building period [denoted $S_a(T_1)$] as the principal IM. A suite of acceleration histories are selected and scaled to be compatible with the site hazard.

The second step involves a suite of nonlinear response history analyses of a structural model of the facility to evaluate its response in terms of engineering demand parameters (EDPs), such as peak interstorey drift, peak floor acceleration, and peak plastic hinge rotation, conditioned on IM. The collapse potential of the structure is evaluated at this stage. The third step, the damage analysis, uses fragility functions that express the conditional probability that a component (e.g. beam, column, wall partition, etc.) is in, or exceeds, a particular damage state. The selected damage states reflect the repair efforts needed to restore the component to an undamaged state. The final step of PBEE establishes the probabilistic losses, which may include repair cost, repair duration, and loss of life.

We apply this methodology to eight alternative layouts of a reinforced-concrete (RC) special moment-resisting frame (SMRF) building, referred to herein as the benchmark structure. Our objectives are both to illustrate the application of the PBEE methodology and to evaluate the expected performance of similar structures designed and constructed in accordance with modern building code provisions. Uncertainties are included and propagated through each step of the PBEE process.

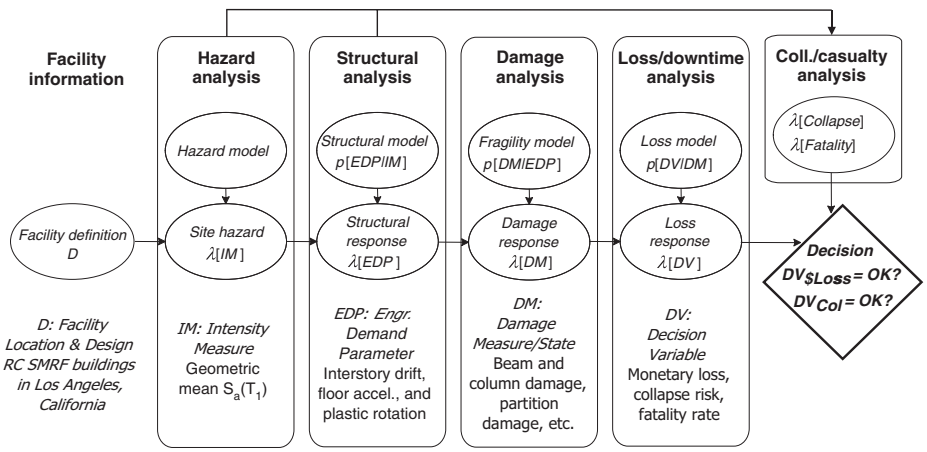


Figure 1. Schematic of PBEE methodology [1].



DOI: 10.1002/eqe

Uncertainty in the factors affecting ground motions is accounted for through probabilistic seismic hazard analysis (PSHA). EDP distributions evaluated from the structural response simulations reflect record-to-record variability, that is, the uncertainty remaining only when the shaking intensity is known. Structural modelling uncertainties are not included in the damage and repair-cost analyses for the non-collapse cases, but they are included for collapse predictions, where they are shown to have a significant effect. The damage and loss analyses treat all the uncertainties in DM given EDP, and DV given DM.

## 2. SITE SELECTION AND DESCRIPTION

The benchmark structure is located on deep sediment near the centre of the Los Angeles basin, at 33.996°N, 118.162°W, south of downtown Los Angeles. The site is within 20 km of seven known faults, but no single major fault produces near-fault motions that dominate the site hazard. High-quality geotechnical data are available for this site from the ROSRINE program [2] according to which the upper 30 m consist of sands and silts with traces of clay and cobbles with an average shear wave velocity $V_{s-30} = 285$ m/s (NEHRP soil category D).

## 3. BENCHMARK BUILDING DESIGN

### *3.1. Structural design*

Figure 2 shows the perimeter-frame variants of the benchmark building, which is a four-storey RC frame structure designed according to the 2003 International Building Code [3]. The space-frame variants are similar, but have moment-resisting frames on every grid line. To represent the likely variation in design assumptions for a modern building of this size, eight designs are considered, as shown in Table I. This set of designs have variation in structural system (space *versus* perimeter), beam strength (25 and 0% additional strength), strong-column weak-beam ratio (code minimum, and 10% additional column strength), and other factors [4]. Seven of these designs are code conforming; an additional design was chosen to investigate the importance of the strong-column weak-beam design provision [5].

The building was designed for a seismic coefficient (ratio of lateral force to building weight) of $C_s = 0.094$. The computed fundamental periods of the seven designs range from 0.53 to 1.25 s.

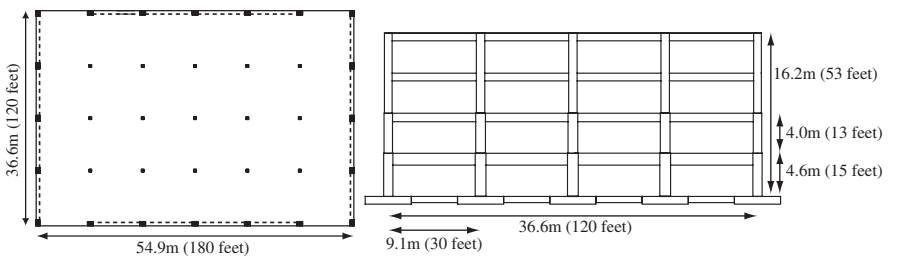


Figure 2. Plan and elevation of the perimeter-frame designs of the four-storey office benchmark building. The space-frame designs are similar, but have moment-resisting frames on each grid line.



DOI: 10.1002/eqe

Table I. Summary of design variants and related design decisions (details in [6]).

| Design | Frame system | Beam design strength factor ($\phi M_n/M_u$) | SCWB factor (code requirement is 1.2) | Provided ratio of positive to negative beam flexural capacity (ACI 318-05 21.3.2.2) | Beams designed as T-beams? | SCWB provision applied in design | Slab steel |
|---|---|---|---|---|---|---|---|
| A | Perimeter | 1.25 | 1.3 | 0.75 | No | 2003 IBC/ACI 318-02 | 2 #4@12″ o.c. |
| B | Perimeter | 1.25* | 1.3* | 0.75* | No | 2003 IBC/ACI 318-02 | 2 #4@12″ o.c. |
| C | Perimeter | 1.0 | 1.2 | 0.5 | No | 2003 IBC/ACI 318-02 | 2 #4@12″ o.c. |
| D | Perimeter | 1.0 | n/a | 0.5 | No | None† | 2 #4@12″ o.c. |
| E | Space | 1.0 | 1.2 | 0.5 | No | 2003 IBC/ACI 318-02 | 2 #4@12″ o.c. |
| F | Space | 1.0 | 1.2 | 0.5 | Yes | 2003 IBC/ACI 318-02 | 2 #4@12″ o.c. |
| G | Space | 1.0 | 1.2 | 0.5 | No | 1997 UBC [5] | 2 #4@12″ o.c. |
| H | Space | 1.0 | 1.2 | 0.5 | No | 1997 UBC [5] | #5, #6@16″ o.c. |

*Only the second floor beam and first-storey columns were proportioned for these ratios; the beams/columns are uniform over the building.

†Columns designed for strength demand and not for strong-column weak-beam (SCWB); this is not a code-conforming design.




DOI: 10.1002/eqe

Element strengths were controlled by the strength demands and the strong-column weak-beam requirement, while sizes were controlled by joint shear capacity provisions, and to a lesser extent, drift limitations. To give a sense for the element sizes, design A has 76 cm × 76 cm (30 in × 30 in) exterior bottom-storey columns with 2.7% longitudinal reinforcement, and 76 cm × 102 cm (30 in × 40 in) interior bottom-storey columns with 1.9% reinforcement. For comparison, design E has smaller 61 cm × 76 cm (24 in × 30 in) exterior columns with 1.7% reinforcement, and the same size interior bottom-storey columns with 1.9% reinforcement. Full design documentation can be found in [6].

For each structural design, a two-dimensional analysis model of a four-bay frame was created. For the perimeter-frame systems, the gravity system was modelled using an equivalent gravity frame in series. The two-dimensional model inherently neglects biaxial bending effects in the columns; to offset this simplification, the space frame columns were designed only for flexural demands in one direction.

### *3.2. Non-structural design: building components considered in loss estimates*

A representative layout and inventory of non-structural and structural elements characteristic of an office building were developed for the purpose of estimating damage and repair costs to structural members, partitions, ceilings, glazing, piping, HVAC (heating, ventilating and air conditioning) system, and other building-specific components [6]. Beck *et al.* [4] show that the building components that contribute the most to repair cost are structural members, drywall partitions and interior paint, which is consistent with our findings presented below.

## 4. SITE HAZARD AND GROUND MOTIONS

### *4.1. Site hazard characterization*

The ground motion hazard characterization involves two aspects—quantification of the earthquake IM and selection of ground motions consistent with the hazard. A PSHA was performed to characterize IMs for seven hazard levels. The PSHA considered several sources of modelling uncertainty, including alternative ground motion prediction equations and alternative estimates of fault slip rate [6]. Plate 1(a) shows mean uniform hazard spectra ('mean' referring to the weighted average over the previously mentioned sources of modelling uncertainty) for three of the seven hazard levels (results for all hazard levels are presented in [6]). Using a nominal first-mode building period of $T_1 = 1.0$ s, spectral accelerations for the seven hazard levels at $T_1$ are $[0.10, 0.19, 0.26, 0.30, 0.44, 0.55, 0.82]g$.

### *4.2. Strong-motion record selection methodology*

Records were selected from the PEER strong motion database [7] that are compatible with hazard analysis results. Disaggregation of the seismic hazard [8] was performed using the UHS ordinate at $T_1 = 1.0$ s to identify the faults that contribute most substantially to the ground motions at the seven hazard levels. As shown in Plate 1(d), at high hazard levels (e.g. 2% probability of exceedance in 50 years), there are significant contributions from a series of near-field faults producing magnitude 6–7 earthquakes at a distance of 10–20 km, as well as San Andreas events of magnitude 7–8 at



DOI: 10.1002/eqe

distance 50–60 km. At lower hazard levels, many magnitude and distance bins contribute similarly to the estimated ground motion (Plate 1(b) and (c)).

In addition to magnitude and distance, the disaggregation was performed on $\varepsilon$ ('epsilon'), which is a period-dependent quantity that measures the normalized offset of spectral acceleration at a given period [($S_a$)] from the median that is expected from ground motion prediction equations

$$\varepsilon = \frac{\ln(S_a) - \mu_{S_a}}{\sigma_{S_a}} \tag{1}$$

where $\mu_{S_a}$ and $\sigma_{S_a}$ are predicted values of the median and standard deviation (in lognormal units) of $S_a$ from these predictions. Baker and Cornell [9] have shown that $\varepsilon$ is a predictor of spectral shape that can significantly affect nonlinear structural response among ground motion records with the same $S_a(T_1)$ value. These dependencies occur because $\varepsilon$ correlates with spectral shape, with high positive $\varepsilon(T_1)$ correlating with a peak in the acceleration spectrum at $T_1$. When scaling the ground motions to a target $S_a(T_1)$ value, an earthquake that has a peak in the acceleration spectrum at $T_1$ is less damaging to a ductile building because of the reduction of spectral acceleration that occurs as period elongates past the peak.

At high hazard levels (Plate 1(d)), the disaggregation results reveal large positive epsilon values ($\varepsilon > 1$) for both the near-field, low-magnitude events and the far-field San Andreas events. This occurs because the return period of the earthquakes on those sources is much lower than the return period of the ground motion. Hence, large $\varepsilon$ (i.e. a rare ground motion realization) is needed to produce the large ground motion associated with these high hazard levels. For relatively low hazard levels (Plate 1(b)), nearby sources with higher magnitudes are characterized by relatively low, often negative, $\varepsilon$ values. This occurs because large magnitude earthquakes on nearby faults are likely to exceed a low ground motion level (i.e. the median from these sources exceeds the ground motion level), thus producing negative $\varepsilon$.

While the disaggregation results in Plate 1 strictly apply for a spectral period of 1 s, very similar results are obtained for the range of first-mode periods for the benchmark building design variants (with periods between 0.53 and 1.25 s). For example, at the 10% in 50 years hazard level, the mean $\varepsilon$ values go from 1.2, 1.3 and 1.4 for the 0.5, 1 and 1.25 s periods, respectively, whereas the magnitude–distance distributions are negligibly affected. These variations are sufficiently small that they do not affect record selection.

For each of the seven hazard levels, independent suites of acceleration histories were selected to represent the site hazard. The records populating each of these seven suites were selected to be consistent with several aspects of the site hazard. First, records were sought that were compatible with the magnitude, distance, and epsilon disaggregation. All selected records were from deep soil sites. For sources at close distance (<35 km), records with appropriate rupture directivity conditions were selected to be consistent with disaggregation results (details in [6]). Records were selected based on the geometric mean of the two horizontal components, which is consistent with the ground motion prediction equations used in PSHA. Accordingly, each record pair provides two horizontal acceleration histories for use in structural simulations. All the selected records within a suite for a given hazard level were scaled such that their geometric mean matched the hazard-specific target $\{S_a(T_1)\}_{\text{target}}$. The average spectra of the selected records after scaling is shown in Plate 1(a) along with the uniform hazard spectra. For a given hazard level, the two spectra match at $T_1 = 1.0$ s, but deviate at other periods due to the spectral shape inherent to the scenario event



DOI: 10.1002/eqe

identified from disaggregation. For example, at high hazard levels, positive $\varepsilon$ values provide mean spectra that are significantly lower than the uniform hazard spectra for periods $>T_1$.

## 5. STRUCTURAL MODELLING AND SIMULATION

### *5.1. Overview of modelling*

PBEE requires structural models to be accurate for relatively low level, frequent ground motions (which contribute most to damage and financial loss) as well as high level, rare ground motions (which contribute most to collapse risk). For low ground motion intensity levels, cracking and tension stiffening phenomena are important to the response of RC structures. For very high ground motion intensity levels, deterioration at large deformations leading to collapse is important.

Available element models generally do not accurately represent the full range of behaviour. Therefore, two models are used: a fibre model for low intensity levels (where cracking and initial yielding behaviour governs) and a plastic hinge model to capture strength and stiffness deterioration and collapse. The fibre model consists of fibre beam-column elements with an additional elastic shear degree-of-freedom at each section, finite joint elements with panel shear and bond-slip springs, and column-base bond-slip springs. The plastic hinge model also includes the joint element, but the beam-column element lumps the bond slip and beam column yielding response into one concentrated hinge. Due to modern capacity design provisions for RC SMRF buildings [5], we do not expect the joint to control the failure mechanism [6], so we modelled it with a bilinear element which accounts for cracking but not strength loss. Similarly, shear failure is not expected for the elements of RC SMRF buildings, so only flexural damage is modelled.

We used OpenSees for the structural analyses [10]. P-Delta effects are accounted for using a combination of gravity loads on the lateral-resisting frame and gravity loads on a leaning column element. The model includes 6.5% Rayleigh damping anchored to the first and third modal periods [11]. Soil–structure interaction (SSI) was considered in some simulations, including foundation flexibility and damping as well as kinematic effects on ground motions at the foundation level of the building. SSI effects were found to be insignificant [6] and are not discussed further. More detail on all aspects of the structural modelling can be found in [6].

### *5.2. Plastic hinge model for collapse simulation*

As shown in Figure 3(a), plastic hinge models for beam columns have a trilinear backbone curve described by five parameters ($M_y$, $\theta_y$, $K_s$, $\theta_{\text{cap}}$, and $K_c$). Figure 3(b) shows an example of calibration of this model to test data; this shows the observed hysteretic response, the calibrated hysteretic response, and the calibrated monotonic backbone curve [12, 13]. This model was developed by Ibarra *et al.* [14] and Ibarra [15]. The negative branch of the post-peak response simulates strain-softening behaviour associated with phenomena such as concrete crushing and rebar buckling and fracture; the accuracy of the onset and slope of this negative branch is the most critical aspect of collapse modelling [6, 14, 15]. The model captures the four important modes of cyclic strength and stiffness degradation; this is based on an energy dissipation capacity and a term that describes how the deterioration rate changes as damage accumulates.

Model parameters for RC beam columns are based on recommendations from Fardis and Biskinis [16] and Panagiotakos and Fardis [17] (for initial stiffness and deformation capacity) and from



DOI: 10.1002/eqe

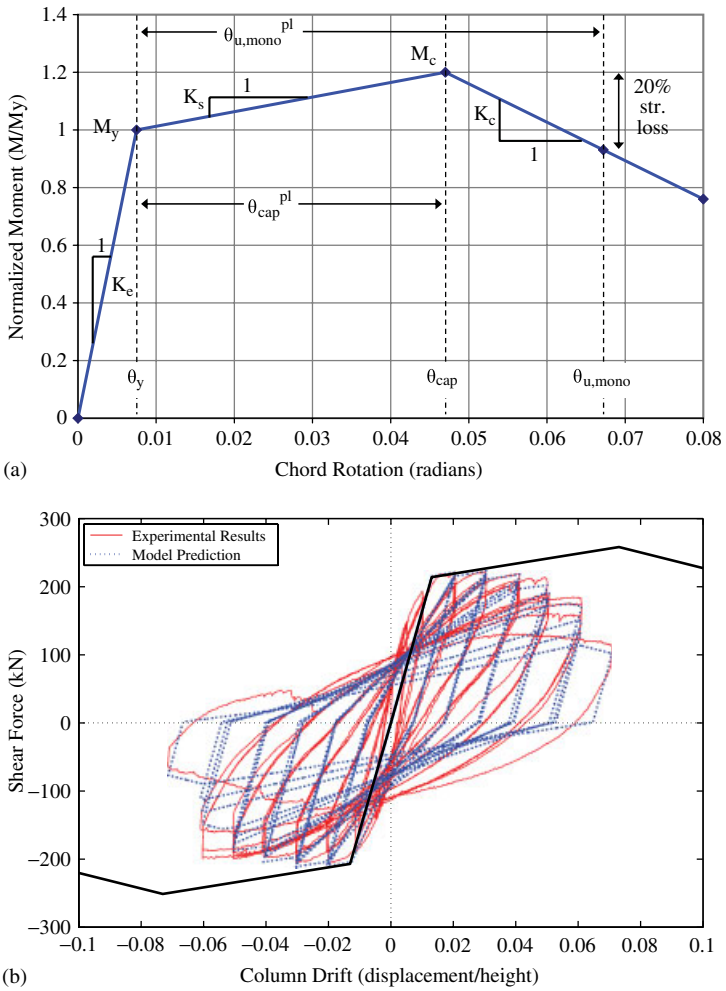


Figure 3. Illustration of spring model with degradation: (a) monotonic backbone curve and (b) observed and calibrated responses for experimental test by Saatcioglu and Grira, specimen BG-6 [12], solid black line is calibrated monotonic backbone. Calibration completed as part of the benchmark study [6] and a more extensive calibration study [13].

our own calibrations to test data using the PEER structural performance database [6, 18] which was developed by Berry and Eberhard. The modelling parameters are briefly summarized here, but [13] includes the most updated and complete element modelling recommendations.

Typical mean capping rotations are $\theta_{\text{cap}}^{\text{pl}} = 0.05$ radians for columns and $\theta_{\text{cap}}^{\text{pl}} = 0.07$ radians for slender beams, with a coefficient of variation of 0.60. These relatively large plastic rotation capacities result from low axial loads, closely spaced stirrups providing shear reinforcement and confinement, and bond-slip deformations.

Initial stiffness of plastic hinges ($K_e$) is defined using both the secant stiffness through the yield point (i.e. $K_e$ taken as $K_{\text{yld}}$) and the secant stiffness through 40% of the yield moment (i.e. $K_e$ taken



DOI: 10.1002/eqe

as $K_{stf}$). Stiffness values $K_{yld}$ and $K_{stf}$ are estimated using both predictions from Panagiotakos and Fardis [17] and calibrations from the PEER database [6, 13, 18]. For example, Panagiotakos and Fardis [17] predict an average $K_{yld}$ of $0.2EI_g$ for low levels of axial load. Our calibrations show that $K_{stf}$ is about twice $K_{yld}$, and the mean inelastic hardening and softening slopes of $K_s/K_{yld} \approx 4\%$ and $K_c/K_{yld} \approx -8\%$, respectively. Our calibrations also provided guidance for cyclic deterioration parameters [6, 13].

### 5.3. *Static pushover analysis*

Static pushover analyses were performed to investigate the general load–deflection relationship for the benchmark building and the sensitivity of results to various modelling assumptions (fibre model *versus* plastic hinge model; use of $K_{yld}$ *versus* $K_{stf}$ for initial stiffness). These analyses were performed using a static lateral force distribution consistent with seismic design provisions [19]. Figure 4(a) shows an illustration for design A (see Table I). The pushover illustrates a few important differences in model predictions: (a) the plastic hinge model using $K_{stf}$ agrees well with the fibre model for low levels of drift; (b) the plastic hinge model using $K_{yld}$ agrees well with the yield drift of the fibre model; (c) the fibre model is less numerically stable and stops converging at 3% roof drift; and (d) the plastic hinge model is capable of capturing strain-softening behaviour that the fibre model cannot.

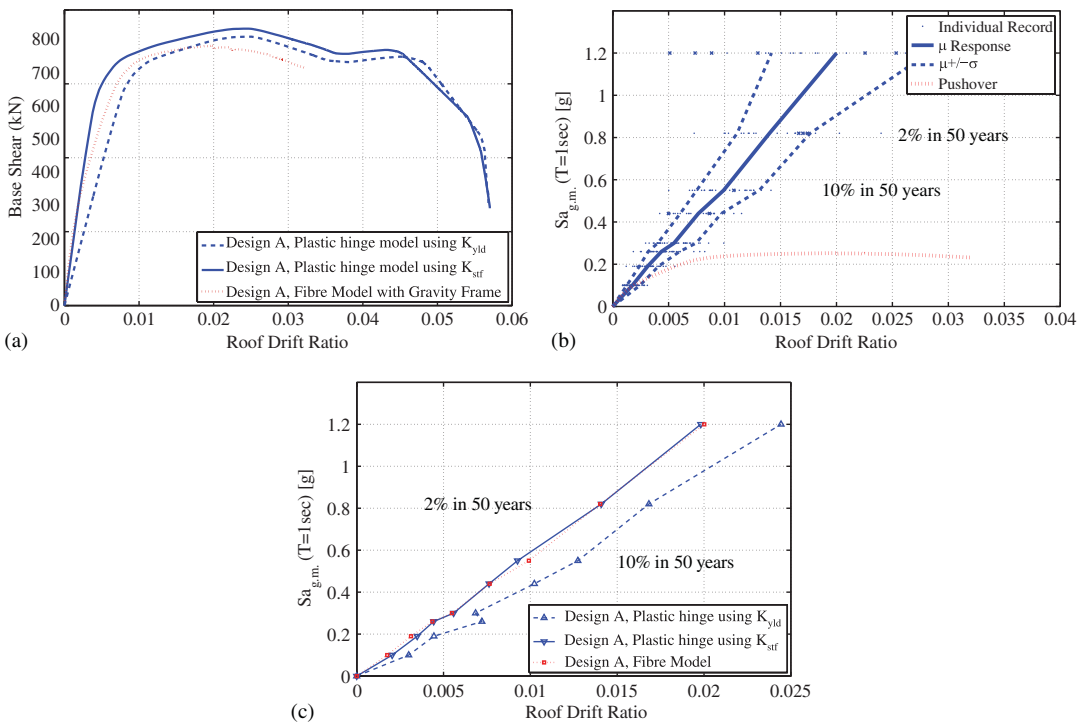


Figure 4. (a) Static pushover curves for both plastic hinge and fibre models; (b) nonlinear dynamic analysis predictions of roof drift ratio for design A using fibre model; and (c) comparison of peak roof drift ratio predictions using the fibre and plastic hinge models for design A.



DOI: 10.1002/eqe

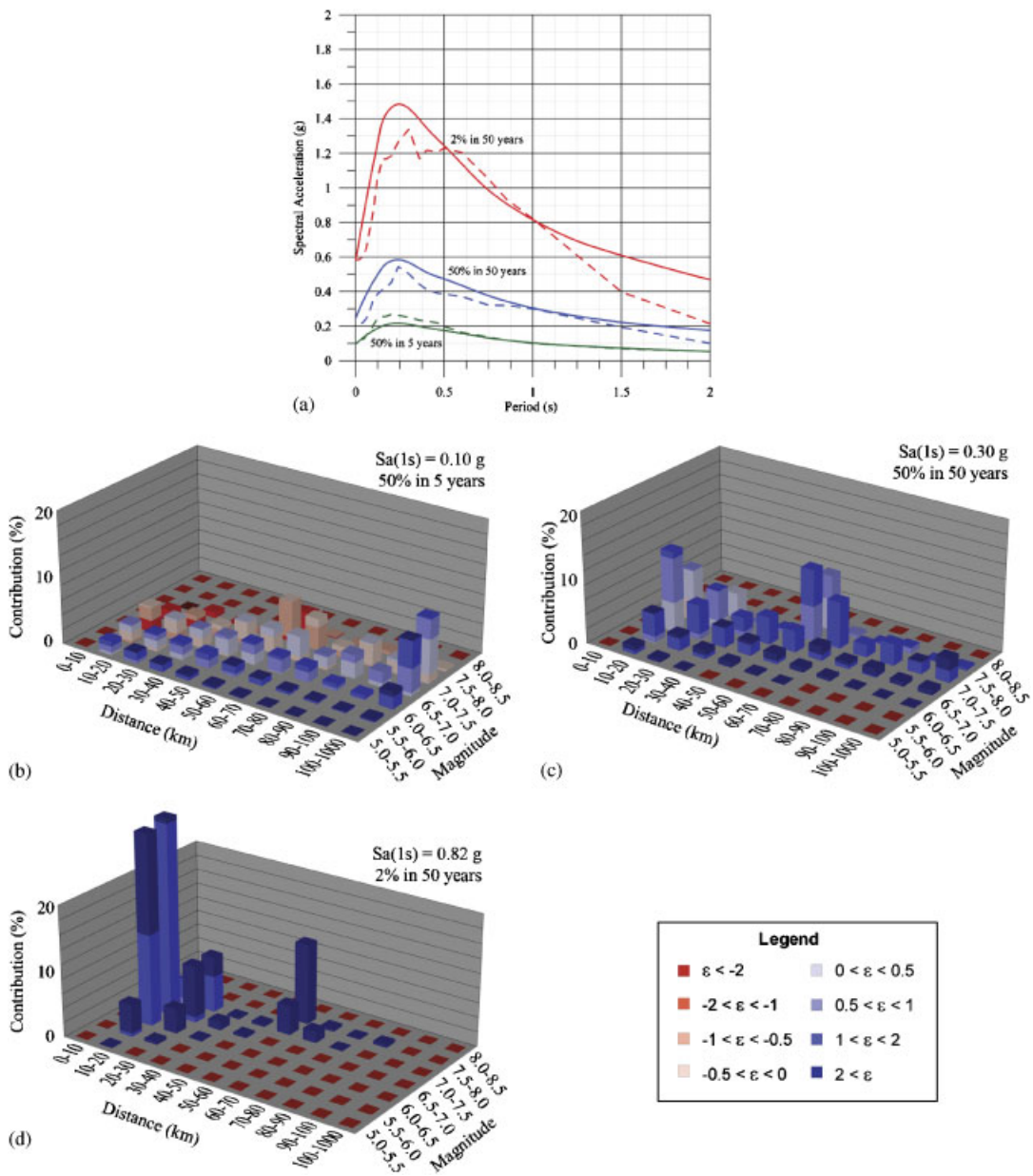


Plate 1. (a) Mean uniform hazard spectra (5% damping) for the LA Bulk Mail site for three selected hazard levels. Continuous lines are the mean spectra from PSHA; dashed lines are the average spectra of the records selected for the corresponding hazard level. (b)–(d) Disaggregation of hazard for three hazard levels at $T = 1.0$ s.



DOI: 10.002/eqe

### *5.4. Nonlinear dynamic analysis—pre-collapse response*

Nonlinear dynamic analyses were performed for the benchmark building designs using ground motion suites for each of the seven selected intensity levels (three are shown in Plate 1(a)), with an additional intensity level of 1.5 of the 2%-in-50-year ground motion. Figure 4(b) shows results for the fibre model while Figure 4(c) compares the fibre model to the plastic hinge model with the two definitions of effective initial stiffness. The static pushover, converted to equivalent spectral acceleration, is also shown for reference [20].

The results in Figure 4(b) and (c) show the roof drift ratio plotted as a function of geometric mean $S_a(T_1)$. The small dots represent the responses from each ground motion component; and the solid and dashed lines represent the mean and mean $\pm$ 1 standard deviation (assuming a lognormal distribution) responses. Figure 4(b) shows that mean roof drift ratios are 1.0 and 1.4% for the 10%- and the 2%-in-50-year ground motion levels, respectively.

This figure also shows that the *mean* dynamic analysis results obey the equal displacement rule[‡] up to the 2% roof drift-level demands, corresponding to shaking 1.5 times larger than the 2%-in-50-year level.

Figure 4(c) compares the mean roof drifts predicted using the fibre and plastic hinge models with the two treatments of initial stiffness. The results show that the plastic hinge model can predict roof drifts consistent with the fibre model only when the larger effective initial stiffness ($K_{stf}$) is used. The lower stiffness ($K_{yld}$) results in an increase of roof drift by 20–25%, which affects monetary loss predictions, as shown below. The larger initial stiffness definition ($K_{stf}$) should be used in the plastic hinge model for the drift predictions to be consistent with those of the fibre model.

### *5.5. Nonlinear dynamic analysis—collapse simulation*

To investigate sidesway collapse, incremental dynamic analyses (IDA) [21] were performed for the benchmark designs. IDA involves increased amplitude scaling of individual ground motion records to estimate both: (a) the relationship between IM (in this case $S_a(T_1 = 1.0\text{ s})$) and EDP; and (b) the IM level that causes sidesway collapse; this study uses IDA only for predicting this collapse IM level. With the goal to evaluate collapse performance, the IDA was performed using the 34 records chosen for the 2%-in-50-year level. Collapse behaviour at ground motion levels stronger than the 2%-in-50-year level can only be simulated using IDA, because we lack records for these less-frequent ground motions.

For the IDA simulations, sidesway collapse is defined as the point of dynamic instability when interstorey drift increases without bound. Figure 5(a) shows IDA results from all 68 ground motion components (34 records with two components each), while Figure 5(b) shows the results obtained using only the horizontal component of each record pair that first causes collapse; results in these figures are for design A. The governing component results from the two-dimensional analyses (Figure 5(b)) are considered reflective of the building collapse behaviour, assuming that the actual (three-dimensional) building will collapse in the more critical of two orthogonal directions when

[‡] The equal displacement rule says that the displacement of the nonlinear structure is equal to that of a linear elastic structure subjected to the same ground motion. This rule typically holds for structures that maintain a positive post-yield stiffness and do not have a short period.



DOI: 10.1002/eqe

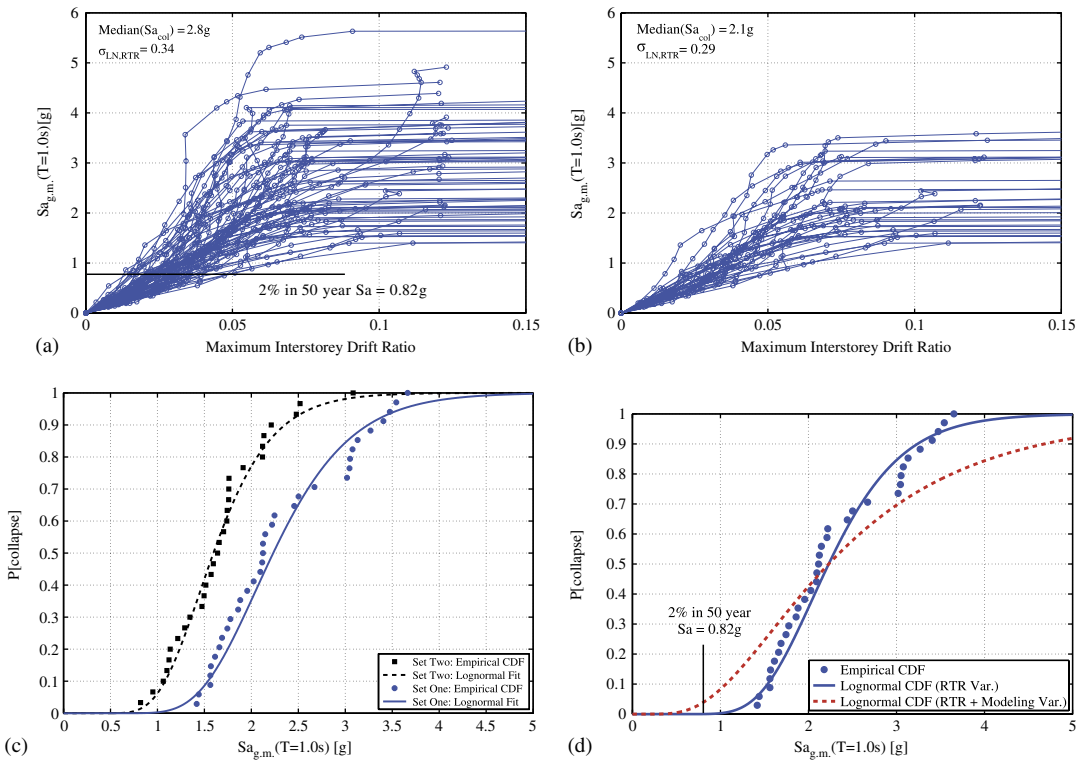


Figure 5. Incremental dynamic analysis for design A, using: (a) both horizontal components of ground motion; (b) the horizontal component that first causes collapse; (c) effect of epsilon (spectral shape) on collapse capacity; and (d) collapse CDFs including and excluding modelling uncertainty.

subjected to the three-dimensional earthquake ground motion.[§] Comparison of Figure 5(a) and (b) shows a 30% lower median collapse capacity ($S_{a_{col}}$), and a 20% lower dispersion ($\sigma_{LN,RTR}$), when only the more critical horizontal ground motion component is used.

*5.5.1. Effects of spectral shape (epsilon).* The results shown in Figure 5(a) and (b) are for the ground motion suite developed above for the 2%-in-50-year ground motion level, in which $\varepsilon$ is accounted for during the selection process; this is termed 'Set One' and the mean value of $\varepsilon(1\text{ s})$ is 1.4 for this data set. We also selected an alternative ground motion record set and performed additional analyses to investigate the effect of $\varepsilon$ on the predicted collapse capacity; this 'Set Two' was selected without regard to $\varepsilon$ and has a mean $\varepsilon(1\text{ s}) = 0.4$.

The collapse $S_a(T_1)$ capacities from Figure 5(b) are plotted as a cumulative distribution function (CDF) in Figure 5(c) (Set One). Superimposed in Figure 5(c) are similar collapse capacities from

[§] This approximate method considers only the differences between the two horizontal components of ground motion, not three-dimensional structural interactions (for the buildings considered in this study, three-dimensional effects should not be significant for perimeter frames, but would be significant for space frame designs).



DOI: 10.1002/eqe

an IDA using ground motions with lower $\varepsilon$ (Set Two). Figure 5(c) shows that a change from Set One to Set Two decreases the expected (median) collapse capacity by 20%, meaning that if one ignores epsilon, one would underestimate collapse capacity. A similar comparison using both horizontal components of ground motion on the benchmark structure instead shows a 40% shift in the median.

Two recent studies provide a comparison to the results shown here. Zareian [22] found that a change from $\varepsilon = 0$ to $+2.0$ caused an approximate 50–70% increase in the expected collapse capacity. Haselton and Baker [23] found that a change consistent with Set One *versus* Set Two causes a 50% shift in median collapse capacity. Results from both of the above studies are comparable with the 40% median shift found in this study.

This shift in the collapse capacity CDF profoundly affects the mean rate of collapse, which depends on the position of the collapse CDF with respect to the hazard curve. For this building where the extreme tail of the hazard curve dominates the collapse rate, a 20% increase in the median collapse capacity causes the mean annual frequency of collapse to decrease by a factor of 5–7 [24]. Similarly, a 40% increase in capacity would decrease the mean annual frequency of collapse by a factor of around 10. These results demonstrate the importance of ground motion acceleration history selection criteria in accurately predicting building collapse capacity.

*5.5.2. Effects of structural modelling uncertainties.* The collapse capacity CDF using Set One ground motions is re-plotted as the solid line in Figure 5(d), where the data points and fitted CDF are for analyses that only reflect the record-to-record variability. The variability in collapse capacity arising from uncertain structural properties was also investigated, and this section explains how we developed the dashed CDF in Figure 5(d).

Table II summarizes the structural parameters for which uncertainties were considered in the dynamic response analyses. Many of these parameters were previously defined in Figure 3(a). Table II shows that variations in some of the parameters are large (e.g. the coefficient of variation in the plastic rotation capacity and degradation parameters is on the order of 0.5–0.6). The first-order second-moment method [25] was used to propagate these structural uncertainties and to estimate the resulting uncertainty in collapse capacity. Correlations between the uncertain structural parameters were considered and found to be important. Using reasonable correlation assumptions, the uncertainty in collapse capacity is a standard deviation of 0.5, in natural log units. This rather large value reflects the large variation in some of the underlying modelling parameters that significantly affect the collapse simulation (Table II). The primary factors that drive the 0.5 value is the uncertainty in element plastic rotation capacity and the correlations among modelling parameters for a given element as well as element-to-element correlations in properties [6].

To incorporate the effects of structural uncertainties, we use the mean estimate method, in contrast to an estimate at a given level of prediction confidence, which effectively combines both record-to-record and structural variability into a single aggregate value. This results in a total log standard deviation of 0.58; this is indicated by the dashed line in Figure 5(d). We offer this value cautiously, since it is based on a first-order approximation and only design A. We believe that further study is required to confirm or improve our estimate.

Even though the mean estimate method does not result in a shift in the median collapse point, the increased variation has a significant effect on collapse probabilities in the lower tail of the distribution. For example, at the 2%-in-50-year ground motion level, the probability of collapse is 0–2% with only record-to-record variability and 2–7% when structural modelling uncertainties are also included. We also compute a mean annual frequency of collapse ($\lambda_{\text{collapse}}$) by numerically



DOI: 10.1002/eqe

Table II. Summary of random variables considered when estimating the uncertainty in collapse capacity resulting from structural uncertainties (references can be found in [6]).

| Structural random variable | Mean | Coefficient of variation |
|---|---|---|
| *Design variables* | | |
| Strong-column weak-beam design ratio | 1.1 ∗ (required) | 0.15 |
| Beam design strength | 1.25 ∗ ($M_u/\varphi$) | 0.20 |
| *System level variables* | | |
| Dead load and mass | 1.05 ∗ (computed[†]) | 0.10 |
| Live load (arbitrary point in time load) | 12 psf | * |
| Damping ratio | 0.065 | 0.60 |
| *Beam-column element variables* | | |
| Element strength ($M_y$) | 1.0 ∗ (computed[‡]) | 0.12 |
| Element initial stiffness ($K_e$) | 1.0 ∗ (computed[§]) | 0.36 |
| Element hardening stiffness ($K_s$) | 0.5 ∗ (computed[‡]) | 0.50 |
| Plastic rotation capacity ($\Theta_{cap}^{pl}$) | 1.0 ∗ (computed[¶]) | 0.60 |
| Hysteretic energy capacity (normalized) ($\lambda$) | 110 | 0.50 |
| Post-capping stiffness ($K_c$) | $-0.08(K_{yld})$ | 0.60 |

*The random variable was treated deterministically.
[†]Computed consistent with common practice.
[‡]Computed using fibre analysis with expected values of material parameters.
[§]Computed using [19] and calibrations from [6].
[¶]Computed using empirical equation from [19].

integrating the collapse CDF with the hazard curve (Equation 7.10 of [15]) (this is the *mean estimate* of the mean annual frequency of collapse). As shown in Table III, inclusion of the structural uncertainties increases $\lambda_{collapse}$ for design A by a factor of 7.5. Hence, proper consideration of structural parameter uncertainties is crucial when evaluating collapse probability and rate.

*5.5.3. Nonlinear dynamic collapse mechanisms.* Figure 6 shows the various collapse mechanisms predicted by nonlinear dynamic analysis. As shown in the figure, there are six types of failure modes, depending on the ground motion record. Note that the static pushover analyses with an inverted triangular loading pattern produces collapse mode (*c*), which occurs in less than 20% of the dynamic analyses.

*5.5.4. Collapse risk predictions for all designs.* Table III summarizes the collapse predictions using the above approach, for all eight designs and modelling variants. Columns 2–4 report the median collapse capacities and parameters of the fitted lognormal distributions. Other columns of this table report collapse probability conditioned on the 2%-in-50-year ground motion level, and the mean rate of collapse ($\lambda_{collapse}$). Results are presented with and without structural modelling uncertainties. Excluding modelling uncertainties, the probabilities of collapse are 0–2% for the 2%-in-50-year ground motion level and mean annual frequencies of collapse are $[0.1–0.5] \times 10^{-4}$; if modelling uncertainties are included, these values increase to 2–7% and $[0.4–1.4] \times 10^{-4}$, respectively. Given these estimates of collapse risk, the question becomes: Is this level of collapse risk acceptable?



DOI: 10.1002/eqe

Table III. Summary of collapse predictions (mean estimates) for all design variants; showing the probability of collapse, annual frequency of collapse, and effects of modelling uncertainty.

| | | | With only record-to-record variability | | | With record-to-record and modelling uncertainty (mean estimate approach) | | | |
|---|---|---|---|---|---|---|---|---|---|
| Design | Median $(S_a, \text{col})[g]$ | $\mu_{\text{LN}(S_a,\text{col})}$ | $\sigma_{\text{LN,RTR}}$ $(S_a, \text{col})$ | $\lambda_{\text{collapse}}$ $(10^{-6})$ | $P[\text{Col}\mid S_{a_{2/50}}]^*$ | $\sigma_{\text{LN,model}}$ $(S_a, \text{col})$ | $\sigma_{\text{LN,Total}(S_a,\text{col})}$ | $\lambda_{\text{collapse}}$ $(10^{-6})$ | $P[\text{Col}\mid S_{a_{2/50}}]^*$ |
| A | 2.19 | 0.86 | 0.36 | 9.2 | 0.00 | 0.45 | 0.58 | 69 | 0.03 |
| B | 2.08 | 0.78 | 0.31 | 9.0 | 0.00 | 0.35 | 0.47 | 38 | 0.02 |
| C | 2.35 | 0.85 | 0.46 | 24.8 | 0.01 | 0.45 | 0.64 | 125 | 0.05 |
| D† | 0.95 | −0.04 | 0.39 | 663.0 | 0.34 | 0.35 | 0.52 | 1300 | 0.38 |
| E | 1.95 | 0.71 | 0.32 | 14.5 | 0.00 | 0.35 | 0.47 | 55 | 0.03 |
| F | 1.86 | 0.57 | 0.38 | 48.1 | 0.02 | 0.35 | 0.52 | 139 | 0.07 |
| G | 1.88 | 0.67 | 0.34 | 20.6 | 0.01 | 0.35 | 0.49 | 71 | 0.04 |
| H | 1.92 | 0.64 | 0.30 | 16.2 | 0.00 | 0.35 | 0.46 | 62 | 0.03 |

*2%-in-50-year ground motion level: $S_a(1\text{ s}) = 0.82g$.

†Columns designed for strength demand and not for SCWB; this is not a code-conforming design.




DOI: 10.1002/eqe

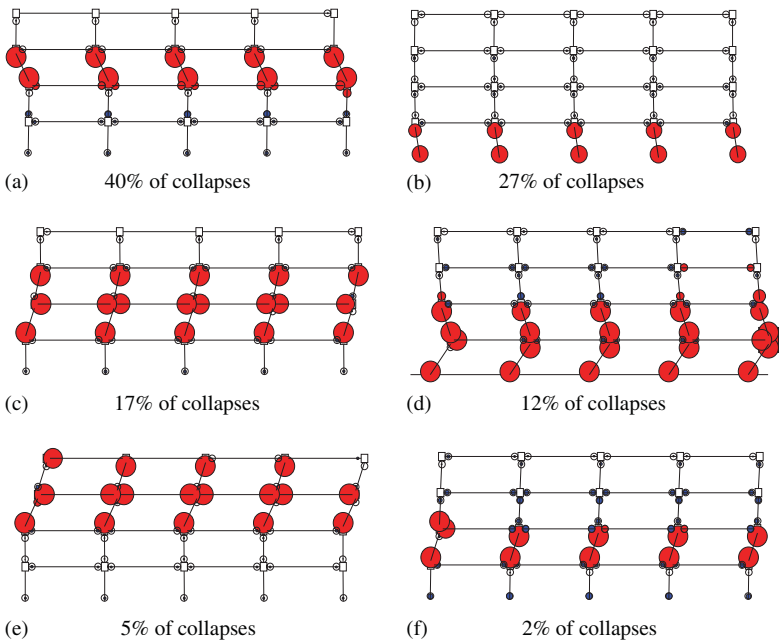


Figure 6. Diagrams showing the collapse modes for design A, and the percentage of ground motion records that caused each collapse mode.

The engineering community should soon come to a consensus on an acceptable collapse risk, so collapse predictions such as these have a consistent basis for comparison.

Design D is equivalent to design B except that the strong-column weak-beam code provision [5] was not imposed in the design. For the 2%-in-50-year hazard level, this building has a 40% probability of collapse (when compared to 2% for code-conforming designs) and a mean annual frequency of collapse of $13 \times 10^{-4}$ (when compared to $[0.4–1.4] \times 10^{-4}$ for code-conforming designs).

## 6. PROBABILISTIC ECONOMIC LOSS ANALYSIS—DIRECT MONETARY LOSS

For the damage and loss analysis, Mitrani-Reiser *et al.* [26] implemented a MATLAB toolbox that was created as part of this benchmark study. The inputs into the toolbox are a database of fragility and cost distribution functions, tables of damageable components, and the hazard and structural analyses results. The outputs of the toolbox are probabilistic descriptions of each damage state for all damageable components in the structure and of some chosen decision variables (DVs). The DVs considered here are the repair costs to restore the building to an undamaged state and the fatality risk.

### *6.1. Fragility and unit-repair-cost functions*

Fragility functions and unit-repair-cost distribution functions are created using experimental data, analytical investigation, expert opinion, or some combination of these. In the loss estimation



DOI: 10.1002/eqe

Table IV. Summary of assembly fragility and cost distribution parameters.

| Assembly description | Unit | EDP | Damage state | Fragility parameters | | Repair-cost parameters | |
|---|---|---|---|---|---|---|---|
| | | | | $x_m$ | $\beta$ | $x_m(\$)$ | $\beta$ |
| Ductile CIP RC beams | ea | DDI | Light | 0.08 | 1.36 | 8000 | 0.42 |
| Ductile CIP RC beams | ea | DDI | Moderate | 0.31 | 0.89 | 22 500 | 0.40 |
| Ductile CIP RC beams | ea | DDI | Severe | 0.71 | 0.80 | 34 300 | 0.37 |
| Ductile CIP RC beams | ea | DDI | Collapse | 1.28 | 0.74 | 34 300 | 0.37 |
| Ductile CIP RC columns | ea | DDI | Light | 0.08 | 1.36 | 8000 | 0.42 |
| Ductile CIP RC columns | ea | DDI | Moderate | 0.31 | 0.89 | 22 500 | 0.40 |
| Ductile CIP RC columns | ea | DDI | Severe | 0.71 | 0.80 | 34 300 | 0.37 |
| Ductile CIP RC columns | ea | DDI | Collapse | 1.28 | 0.74 | 34 300 | 0.37 |
| Column–slab connections | ea | IDR | Light cracking | 0.0030 | 0.40 | 35 | 0.20 |
| Column–slab connections | ea | IDR | Severe cracking | 0.0100 | 0.30 | 435 | 0.20 |
| Column–slab connections | ea | IDR | Punching shear failure | 0.0145 | 0.60 | 3273 | 0.20 |
| Drywall partition | 64 ft$^2$ | IDR | Visible | 0.0039 | 0.17 | 88 | 0.20 |
| Drywall partition | 64 ft$^2$ | IDR | Significant | 0.0085 | 0.23 | 525 | 0.20 |
| Drywall finish | 64 ft$^2$ | IDR | Visible | 0.0039 | 0.17 | 88 | 0.20 |
| Drywall finish | 64 ft$^2$ | IDR | Significant | 0.0085 | 0.23 | 253 | 0.20 |
| Exterior glazing | pane | IDR | Crack | 0.040 | 0.36 | 439 | 0.26 |
| Exterior glazing | pane | IDR | Fallout | 0.046 | 0.33 | 439 | 0.26 |
| Acoustical ceiling | ft$^2$ | PDA | Collapse | $92/(l+w)$ | 0.81 | $2.21 * A$ | 0.50 |
| Automatic sprinklers | 12 ft | PDA | Fracture | 32 | 1.4 | 900 | 0.50 |

DDI, deformation damage index portion of the Park-Ang damage index; IDR, interstorey drift ratio; PDA, peak diaphragm acceleration; $l$, room length; $w$, room width; $A$, room area.

literature, lognormal distributions are commonly used to quantify the uncertainty in the unit repair costs and fragility corresponding to the various damage states for each damageable structural and non-structural assembly [4, 27, 28]. Therefore, the median capacity and logarithmic standard deviations of capacity (defined in terms of the EDP value that causes an assembly to reach or exceed a given damage state) are used to create the fragility functions, and then to estimate damage. The corresponding medians and logarithmic standard deviations of associated unit repair costs for each damage state of an assembly are used to define the unit-repair-cost distribution functions for the loss assessment. Existing and new fragility functions and unit-repair-cost functions that are used in this study are summarized in Table IV, where $x_m$ and $\beta$ denote the median and logarithmic standard deviation, respectively. This table lists the structural and non-structural components of the benchmark building and the EDPs used the damage analysis; additional information for each of these components is available in [6].

### *6.2. Damage analysis*

The structural analysis results are combined with the damageable component fragility functions, using the law of total probability, to compute the probability of reaching or exceeding damage state $j$ for a component of type $i$, conditioned on the structure not collapsing (NC)



DOI: 10.1002/eqe

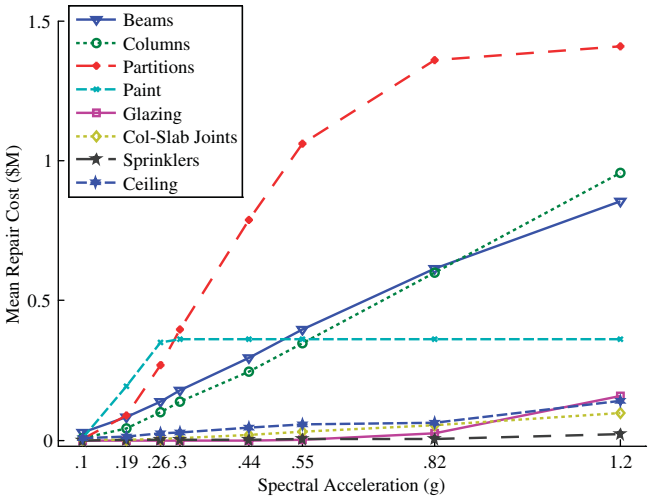


Figure 7. Total repair costs broken down into contributions of cost for each damageable building component for baseline perimeter-frame design (variant #1, design A).

and on IM:

$$P[\mathrm{DM}_{ij}|\mathrm{NC}, \mathrm{IM}] = \int_{\mathrm{EDP}_i} P[\mathrm{DM}_{ij}|\mathrm{EDP}_i]\, p(\mathrm{EDP}_i|\mathrm{NC}, \mathrm{IM})\mathrm{dEDP}_i \tag{2}$$

The first factor in the integrand, $P[\mathrm{DM}_{ij}|\mathrm{EDP}_i]$, is given by the fragility function for damage state $j$ for a building component of assembly type $i$, where $\mathrm{EDP}_i$ is the value of EDP appropriate for assembly type $i$. The second factor in the integrand, $p(\mathrm{EDP}_i|\mathrm{NC}, \mathrm{IM})$, is the probability density function for the appropriate EDP, conditioned on the structure not collapsing and on a given IM level, which is assumed to be lognormally distributed. The required median and standard deviation are estimated from the structural response simulated using the fibre model (Figure 4(b)) and reflects record-to-record variability but not structural modelling uncertainties. The latter are neglected because the probabilities evaluated in Equation (2) involve structural deformation levels for which previous studies have shown that structural uncertainties do not play a significant role [29].

Plate 2 presents an example of the damage prediction for the baseline perimeter-moment-frame design (variant #1, design A), showing the average probability of reaching or exceeding each damage state for like components on each storey level. As expected, the probability of exceeding each damage state increases with increasing IM. The partitions become significantly damaged for $S_a > 0.44g$, where nearly 50% of the partitions show damage that would lead to replacement. The columns are most damaged in the first storey, which could lead to a collapse mechanism as the one shown in Figure 6(b) or possibly Figure 6(d); the beams are most damaged on the third floor, which corresponds to the collapse mechanism shown in Figure 6(c). The results in Figure 7 show that the repairs of wallboard partitions correspond to 21% of the mean total repair cost at $0.19g$, 30% at $0.26g$, 35% at $0.30g$, and 45% at $0.44g$. The damage analysis results for all design variants considered in the benchmark study can be found in [6].



DOI: 10.1002/eqe

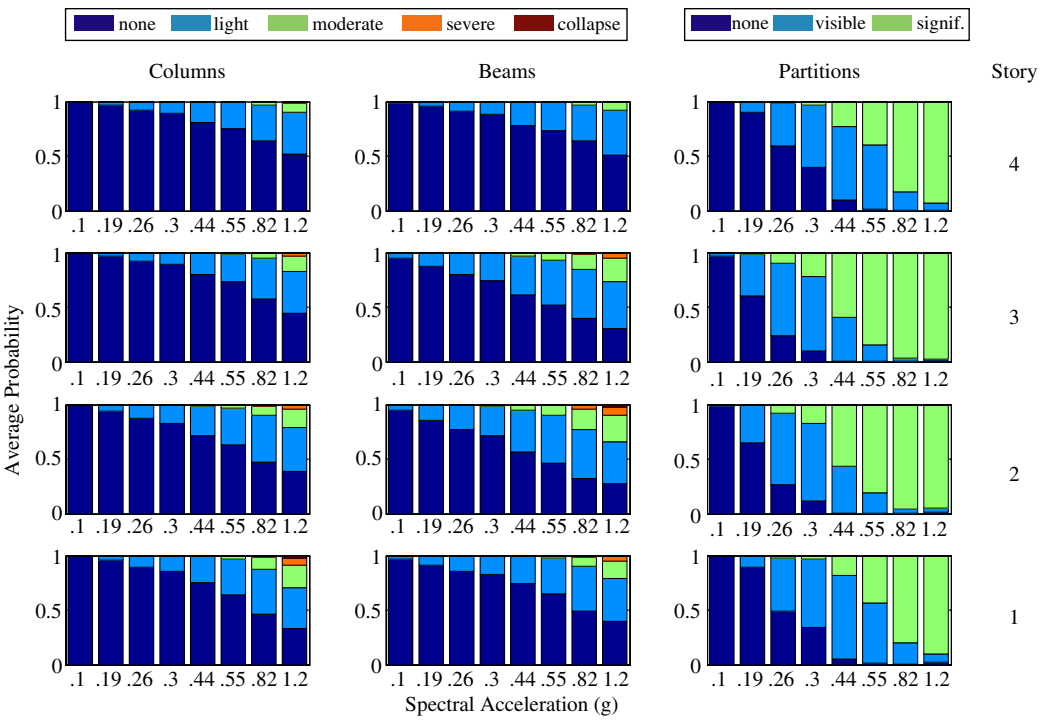


Plate 2. Average probabilities of damage per storey level for baseline perimeter-frame design (variant #1, design A).



DOI: 10.002/eqe

### *6.3. Vulnerability functions*

Vulnerability functions are the probabilistic relationships between repair costs and shaking intensity levels. Using the laws of probability, the mean and variance of the vulnerability function are given by

$$\begin{aligned} E[\mathrm{TC}|\mathrm{im}] &= E[\mathrm{TC}|\mathrm{NC}, \mathrm{im}] \cdot (1 - P[C|\mathrm{im}]) + E[\mathrm{TC}|C, \mathrm{im}] \cdot P[C|\mathrm{im}] \\ E[\mathrm{TC}^2|\mathrm{im}] &= E[\mathrm{TC}^2|\mathrm{NC}, \mathrm{im}] \cdot (1 - P[C|\mathrm{im}]) + E[\mathrm{TC}^2|C, \mathrm{im}] \cdot P[C|\mathrm{im}] \\ \mathrm{var}[\mathrm{TC}|\mathrm{im}] &= E[\mathrm{TC}^2|\mathrm{im}] - (E[\mathrm{TC}|\mathrm{im}])^2 \end{aligned} \tag{3}$$

where $E[\mathrm{TC}|\mathrm{im}]$ is the expected total repair costs conditioned on $\mathrm{IM} = \mathrm{im}$, $E[\mathrm{TC}|C, \mathrm{im}]$ is the replacement cost of the structure, and $P[C|\mathrm{im}]$ is the probability of collapse (including both record-to-record variability and structural modelling uncertainty), which is estimated from the structural response simulated using the plastic hinge model (Table III).

Similarly, $E[\mathrm{TC}^2|\mathrm{im}]$ is the mean square of the total repair costs conditioned on $\mathrm{IM} = \mathrm{im}$ and $\mathrm{var}[\mathrm{TC}|\mathrm{im}]$ is the variance conditioned on $\mathrm{IM} = \mathrm{im}$. The RSMeans Corp. [30] construction cost estimates for mid-rise commercial office buildings, based on the gross square footage of the benchmark building in Los Angeles, CA are: \$7.3M (low), \$8.9M (median) and \$12.1 (high). The median total project cost, \$8.9M (\$103/sf), is used as the replacement cost for the perimeter-frame designs. The RS Means Corp. assemblies cost data [30] can be used to estimate the difference in cost between the building components in the perimeter-frame and space-frame designs. The calculated median replacement cost for the space frame is \$9.0M (\$104/sf). The values for replacement cost may seem low, relative to current market conditions in California, but are presented here for illustration as a rough gauge against which to compare the economic loss results.

The expected total repair cost conditioned on the structure not collapsing and on IM, $E[\mathrm{TC}|\mathrm{NC}, \mathrm{im}]$, is calculated by summing the repair costs of all damageable assembly groups

$$\begin{aligned} E[\mathrm{TC}|\mathrm{NC}, \mathrm{im}] &= (1 + C_{\mathrm{op}}) \cdot C_i \cdot C_L \sum_{i=1}^{\mathrm{na}} N_{\mathrm{u}_i} \cdot E[\mathrm{RC}_i|\mathrm{NC}, \mathrm{im}] \\ E[\mathrm{RC}_i|\mathrm{NC}, \mathrm{im}] &= \sum_{j=1}^{\mathrm{nds}_i} E[\mathrm{RC}_i|\mathrm{DM}_{ij}] \cdot P[\mathrm{DM}_{ij}|\mathrm{NC}, \mathrm{im}] \end{aligned} \tag{4}$$

where $C_{\mathrm{op}}$, $C_i$, $C_L$ are the factors for contractor overhead and profit, for inflation, and for location, respectively; na is the number of damageable assembly groups; $N_{\mathrm{u}_i}$ is the number of units in assembly group $i$; $\mathrm{RC}_i$ is the repair cost for one unit in assembly group $i$; and $\mathrm{nds}_i$ is the number of damage states for damageable component group $i$. Note that each assembly group is composed of damageable components sensitive to the same EDP, and their damage states and repair costs are modelled as perfectly correlated and conditionally independent given EDP from all other assembly groups.

An example of expected repair cost as a function of $\mathrm{IM} = S_{\mathrm{a}}$ is shown in Figure 7, where the cost is broken down into contributions from each damageable component. This figure shows that the contribution of wallboard partitions is significant for all hazard levels and that the contributions of glazing, column–slab connections, sprinkler piping and ceilings do not play a major role in the total repair costs.



DOI: 10.1002/eqe

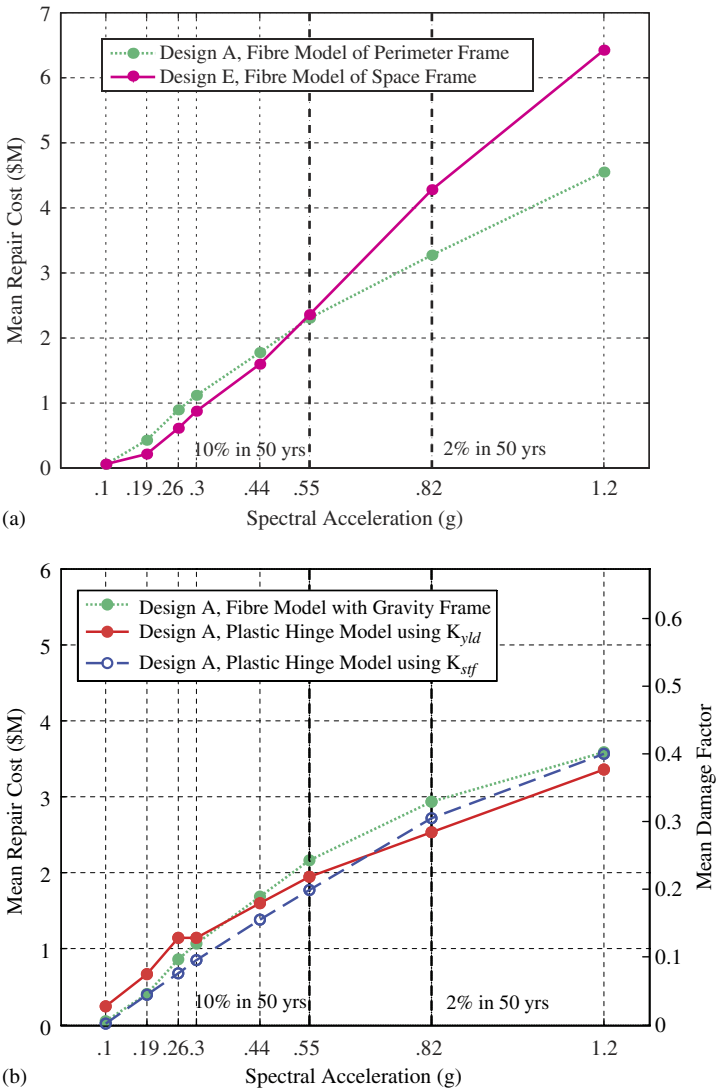


Figure 8. (a) Vulnerability functions for design models A and E (variants #1 and #6), comparing two design choices and (b) vulnerability functions for design A (variants #1, #13, and #15), comparing modelling choices.

Figure 8 shows selected vulnerability functions (using $C_{\text{op}} = 0.175$; $C_i = 1.13$; and $C_L = 1.085$). Figures 8(a) and (b) show the effect that design choices and modelling choices can have on the loss analysis. In Figure 8(a), the curve for variant #1 (dotted line) corresponds to a perimeter-moment-frame baseline design and the curve for variant #6 (solid line) corresponds to the space-frame baseline design. The space-frame design should better withstand lateral motions since it has lateral force-resisting moment frames on every grid line, which is consistent with Figure 8(a) until just before $S_{\text{a}} = 0.55g$. The beams and columns are heavily damaged at the two highest hazard levels



DOI: 10.1002/eqe

for simulation ($S_a = 0.82$ and $1.2g$) and because there are more of them to repair in the space-frame design than in the perimeter-frame design, their contributions to the total repair cost dominate the contributions of the other damageable components. In fact, the contribution to mean total repair cost from the beams surpasses that of the partitions in the space-frame design at all levels of $S_a$, which does not occur in any of the perimeter-frame variants.

In Figure 8(b), the curve for variant #13 (solid line) corresponds to the baseline perimeter-moment-frame design using a plastic hinge model with initial stiffness defined as the secant stiffness through the yield point ($K_{yld}$); the curve for variant #15 (dashed line) corresponds to a similar design except that the initial stiffness is defined as the secant stiffness corresponding to 40% of the yield moment ($K_{stf}$); variant #1 (dotted line) is given again in this plot to compare the baseline fibre model with these plastic hinge models. Note that the fibre model results are consistent with the ones from the plastic hinge model using $K_{stf}$ until $S_a = 0.19g$, where the two curves diverge and the mean total repair costs become greater than for the fibre model for all values of $S_a > 0.19g$. This is consistent with the behaviour shown in the static pushover curves of Figure 4(a). A summary of the variants considered in this study is shown in Table V and the corresponding means and coefficients of variation of the total repair costs are given for each level of $S_a$.

### *6.4. Expected annual loss*

The expected annual loss (EAL) is a valuable result for property stakeholders, which accounts for the frequency and severity of various seismic events. EAL is calculated as the product of the mean total rate of occurrence of events of interest and the mean loss conditional on an event of interest occurring [25, 31], which may be expressed as

$$\mathrm{EAL} = \upsilon_0 \int_{\mathrm{im}_0}^{\infty} E[\mathrm{TC}|\mathrm{im}]\, p(\mathrm{im}|\mathrm{IM} \geqslant \mathrm{im}_0)\, \mathrm{dim} \tag{5}$$

where $\upsilon_0$ is the mean annual rate of events of interest defined by $\mathrm{IM} \geqslant \mathrm{im}_0$; $E[\mathrm{TC}|\mathrm{im}]$ is calculated as in Equation (3) and is shown for some variants in Figure 8; and $p(\mathrm{im}|\mathrm{IM} \geqslant \mathrm{im}_0)$ is the probability density function for IM, given that an event of interest has occurred. For the chosen IM, spectral acceleration, the threshold for events of interest is chosen here as $\mathrm{im}_0 = 0.1g$. Table V shows the EAL results for all variants considered in the previous section. The lowest value (for variant #6, design E) represents about 0.6% of the building value, whereas the largest value (for variant #9, design D) represents about 1.3%.

The collapse risk of the code-conforming buildings can significantly contribute to the 'cost' associated with loss of life. Similar to EAL, expected annual losses due to fatalities (EALF) can be computed using the acceptable cost to avoid a future statistical death [32], a binomial distribution model for fatalities given structural collapse [6], and a fatality probability for building total collapse [33]. The complete procedure is described in [6].

Although many people are uncomfortable with putting a price on human life, and the process is fraught with philosophical and economic challenges, public agencies routinely allocate scarce resources to improve life safety, and for the public good must assess the value of competing activities, regulations, and policies that cost money but save lives [32]. As additional justification for estimating EALF, it must be noted that, to compare purely economic benefits and costs and ignore life safety is to neglect the value of human life entirely.



DOI: 10.1002/eqe

Table V. Design variant descriptions and corresponding EAL results.

| Variant number, design and model description | $S_a(T_1)$ | 0.1 | 0.19 | 0.26 | 0.3 | 0.44 | 0.55 | 0.82 | 1.2 | EAL ($) |
|---|---|---|---|---|---|---|---|---|---|---|
| VID #1 (design A): perimeter frame, designed with expected overstrength; fibre model, concrete tensile strength modelled, gravity frame included | Mean | 0.06 | 0.43 | 0.90 | 1.12 | 1.78 | 2.30 | 3.27 | 4.55 | 66 460 |
| | COV | 0.52 | 0.17 | 0.15 | 0.16 | 0.20 | 0.24 | 0.33 | 0.36 | |
| VID #2 (design C): same as design A, but designed with uniform beams and columns over height; modelled same as VID #1 | Mean | 0.04 | 0.35 | 0.64 | 0.80 | 1.47 | 1.90 | 2.91 | 4.24 | 51 807 |
| | COV | 0.62 | 0.18 | 0.16 | 0.17 | 0.21 | 0.27 | 0.42 | 0.46 | |
| VID #3 (design B): same as design A, but designed with bare code-minimum strengths; modelled same as VID #1 | Mean | 0.10 | 0.71 | 1.34 | 1.44 | 2.08 | 2.54 | 3.42 | 4.38 | 95 530 |
| | COV | 0.37 | 0.13 | 0.12 | 0.12 | 0.11 | 0.13 | 0.23 | 0.35 | |
| VID #6 (design E): baseline space frame; fibre model, concrete tensile strength modelled | Mean | 0.06 | 0.22 | 0.61 | 0.87 | 1.60 | 2.36 | 4.28 | 6.42 | 49 296 |
| | COV | 0.51 | 0.25 | 0.15 | 0.14 | 0.16 | 0.17 | 0.20 | 0.16 | |
| VID #9 (design D): same as design C, but no SCWB provision enforced (not code conforming); modelled same as VID #1 | Mean | 0.13 | 0.80 | 1.51 | 1.64 | 2.62 | 3.40 | 5.31 | 7.17 | 112 810 |
| | COV | 0.36 | 0.33 | 0.40 | 0.51 | 0.64 | 0.66 | 0.53 | 0.34 | |
| VID #11 (design A): same as design A; modelled same as VID #1, but concrete tensile strength and stiffness not modelled | Mean | 0.12 | 0.70 | 1.19 | 1.34 | 2.00 | 2.46 | 3.26 | 4.71 | 92 596 |
| | COV | 0.35 | 0.13 | 0.13 | 0.14 | 0.18 | 0.22 | 0.33 | 0.34 | |
| VID #12 (design A): same as design A; modelled same as VID #1, but gravity frame not modelled | Mean | 0.06 | 0.52 | 1.09 | 1.25 | 1.90 | 2.35 | 3.22 | 4.38 | 75 943 |
| | COV | 0.49 | 0.15 | 0.14 | 0.15 | 0.19 | 0.23 | 0.34 | 0.39 | |
| VID #13 (design A): same as design A; plastic hinge model with secant stiffness through yield ($K_{yld}$) | Mean | 0.26 | 0.69 | 1.19 | 1.19 | 1.69 | 2.06 | 2.74 | 3.72 | 96 153 |
| | COV | 0.17 | 0.15 | 0.15 | 0.16 | 0.22 | 0.28 | 0.44 | 0.49 | |
| VID #14 (design A): same as design A; plastic hinge model, with secant stiffness through 60% of yield | Mean | 0.12 | 0.63 | 1.07 | 1.13 | 1.68 | 2.10 | 3.02 | 4.40 | 82 307 |
| | COV | 0.29 | 0.15 | 0.15 | 0.17 | 0.21 | 0.27 | 0.37 | 0.38 | |
| VID #15 (design A): same as design A; plastic hinge model with secant stiffness through 40% of yield ($K_{stf}$) | Mean | 0.03 | 0.42 | 0.72 | 0.91 | 1.48 | 1.91 | 3.10 | 4.49 | 57 237 |
| | COV | 0.75 | 0.17 | 0.17 | 0.19 | 0.25 | 0.30 | 0.36 | 0.37 | |

Mean, mean total repair cost for $S_a(g)$ in \$M; COV, coefficient of variation of repair cost for $S_a(g)$.

The expected annual number of fatalities for designs A, B, D, and E ranges between 0.001 and 0.004 (EALF = \$4300–\$14 300, respectively), including IMs extrapolated up to $S_a = 4g$. The expected annual number of fatalities increases drastically to 0.05 for design D (consistent with 0.06 reported for a post-Northridge steel moment-resisting frame building [34, 35]), which



DOI: 10.1002/eqe

does not include the SCWB provision. These values of EALF are expected to be conservative (meaning high) because of the various assumptions made, such as full occupancy around the clock and that all collapses are total (rather than some partial).

## 7. CONCLUSIONS

We have implemented a PBEE methodology to predict seismic performance of a four-storey RC SMRF benchmark building that is designed according to the 2003 IBC [3]. Performance is quantified in terms of structural and non-structural damage, repair costs, collapse statistics, and losses due to fatalities. Several design alternatives for the benchmark building are considered along with several structural modelling alternatives for a given design.

Accounting for uncertainties in both structural modelling and record-to-record variability, collapse probabilities lie in the range 2–7% for earthquake ground motions with a 2% probability of exceedance in 50 years. Combining the ground motion hazard with the collapse predictions, we find mean frequencies of collapse of $[0.4–1.4] \times 10^{-4}$ for the various benchmark building designs.

Figure C1-23 from the FEMA 223 document [35] suggests that these computed collapse probabilities are high, compared with previous estimates on the order of 0.2–0.5% for a building subjected to 2%-in-50-year ground motions. The topic of acceptable collapse risk is worthy of substantial further study.

In the process of developing the above findings related to collapse, a number of important considerations were revealed that are likely transferable to other buildings:

- For rare ground motions, it is critical to select ground motion records in consideration of spectral shape. Here, this was done using parameter $\varepsilon$ from the PSHA. If $\varepsilon$ had been neglected in our simulations, the median predicted collapse capacities would be reduced by 20–40%, which in turn increases the mean annual rate of collapse by a factor of 5–10.
- Realistic estimates of plastic rotation capacity are essential for accurate collapse predictions. Recent research and new model calibrations conducted as part of this study reveal much larger rotation capacities, on the order of 0.06 radians for a conforming RC element, than are generally assumed in modern practice (see Section 5.2).
- Collapse probability is highly sensitive to structural modelling uncertainties. The introduction of structural modelling uncertainty increased estimated collapse rates by approximately a factor of 4–8. We believe, therefore, that further study of this issue is critical.
- Different collapse mechanisms occur for different ground motions, and the mechanism predicted by nonlinear static pushover analysis was not the predominant collapse mechanism observed in the time-series response analyses.
- As expected, the structural design that did not enforce the strong-column weak-beam provision collapsed at lower hazard levels than the code-conforming designs. The collapse probability at the 2%-in-50-year ground motion was 38%, when compared to 2–7% for the seven conforming designs. The mean annual frequency of collapse is $13 \times 10^{-4}$ and the mean annual number of fatalities is 0.05, when compared to $[0.4–1.4] \times 10^{-4}$ and to 0.001–0.004, respectively, for the seven conforming designs.

The potential for financial loss is considerable. Loss modelling considering the moment-frame beams and columns, the column–slab connections, the wallboard partitions, the acoustical ceiling, the sprinkler piping, the exterior glazing, and the interior paint, indicates that mean annual losses



DOI: 10.1002/eqe

from earthquakes are likely in the range of \$52 000–\$95 000 for the various code-conforming benchmark building designs, or roughly 1% of the replacement cost of the building. Some important lessons learned from these simulations that may be transferable to other projects include the following:

- Economic losses are dominated by the expected costs of repairing the wallboard partitions, the structural members and painting the interior, in this order of importance (see Figure 7).
- Expected annual loss (EAL) estimates are highly sensitive to the manner of estimating the initial stiffness of the structural elements. The EAL for the baseline perimeter-frame model using the fibre model is \$66 500 (0.75% of replacement cost); the EAL for the same design using the plastic hinge model with secant stiffness through yield ($K_{yld}$) is \$96 200 (1.1% of replacement cost); the EAL using a secant stiffness through 60 and 40% of yield ($K_{stf}$) is \$82 300, and \$57 200, (0.9, and 0.6% of replacement cost), respectively. If a plastic hinge approach is used to model the structural behaviour, the initial stiffness of the hinge element should be calibrated to test data and chosen carefully (similar to $K_{stf}$) to better model the building stiffness under frequent ground motions.
- Losses are sensitive to other modelling choices. If the tensile strength of the concrete is ignored by assuming all pre-cracked concrete (variant #11) (this changes the initial stiffness of the element model), there is an increase of almost 40% in EAL. If the gravity frame is ignored in the structural model (variant #12), thus neglecting the contribution of its strength and stiffness, there is an increase of almost 15% in EAL.
- Variant #2 (design C), a more conservative design than variant #1 (design A) because it uses the same beams and columns throughout the building, produces an EAL that is 22% smaller (Table V). Variant #3 (design B), a code-minimum design, produces an EAL that is 44% larger (Table V).
- The strong-column weak-beam provisions are ignored for variant #9 (design D), which drastically increases the EAL of the baseline model (variant #1, design A) by 70%.
- Although the mean repair costs are much higher for the space-frame designs than for the perimeter-frame designs at the two highest levels of $S_a$ (see Figure 8(a)), the EAL and the expected annual loss from fatalities (EALF) for the space-frame design is 25 and 33% less than the perimeter-frame design, respectively. This is because the mean repair costs are lower for the more frequent events and because the space-frame design has less risk of collapse. These reductions in EAL and EALF can be used to allow stakeholders to make trade-offs between the extra up-front cost (approximately \$100 000) for the space-frame design [6].

## ACKNOWLEDGEMENTS

This work was supported primarily by the Earthquake Engineering Research Centers Program of the National Science Foundation, under award number EEC-9701568 through the Pacific Earthquake Engineering Research Center (PEER). Any opinions, findings, and conclusions or recommendations expressed in this material are those of the authors and do not necessarily reflect those of the National Science Foundation. Supplementary funding was also provided to Christine Goulet from the National Sciences and Engineering Research Council of Canada and from le Fonds québécois de la recherche sur la nature et les technologies. The primary lead institutions for the seismic hazard analysis, the structural analysis, and the damage and loss analysis, in this PEER project are, respectively, the University of California at Los Angeles (J. Stewart (P.I.) and C. Goulet), Stanford University (G. Deierlein (P.I.) and C. Haselton) and the California Institute of Technology (J. Beck (P.I.), J. Mitrani-Reiser and K. Porter). The authors



DOI: 10.1002/eqe

would also like to acknowledge the valuable input from Professors Helmut Krawinkler, Allin Cornell, Eduardo Miranda, Ertugrul Taciroglu and Jack Baker; architect and professional cost estimator, Gee Hecksher; graduate student Abbie Liel; and undergraduate interns Sarah Taylor Lange and Vivian Gonzales at Stanford and Caltech, respectively.

## REFERENCES

1. Porter KA. An overview of PEER's performance-based earthquake engineering methodology. *Proceedings of Ninth International Conference on Applications of Statistics and Probability in Civil Engineering*, San Francisco, CA, 2003.
2. ROSRINE. *Resolution of Site Response Issues from the Northridge Earthquake*. Website by Earthquake Hazard Mitigation Program & Caltrans. http://gees.usc.edu/ROSRINE/ (last accessed January 2007), 2007.
3. ICC. *2003 International Building Code*. International Code Council: Falls Church, VA, 2003.
4. Beck JL, Porter KA, Shaikhutdinov R, Au SK, Mizukoshi K, Miyamura M, Ishida H, Moroi T, Tsukada Y, Masuda M. Impact of seismic risk on lifetime property values. *Report CKIV-03*, *Consortium of Universities for Research in Earthquake Engineering*, Richmond, CA, 2002.
5. ACI. *Building Code Requirements for Structural Concrete* (*ACI 318-02*) *and Commentary* (*ACI 318R-02*). American Concrete Institute: Farmington Hills, MI, 2002.
6. Haselton CB, Goulet C, Mitrani-Reiser J, Beck J, Deierlein GG, Porter KA, Stewart JP, Taciroglu E. An assessment to benchmark the seismic performance of a code-conforming reinforced-concrete moment-frame building. *PEER Report 2007*, University of California, Berkeley, CA, 2007.
7. PEER. *Pacific Earthquake Engineering Research Center*: *PEER Strong Motion Database*. University of California: Berkeley, CA, http://peer.berkeley.edu/smcat/ (last accessed January 2007), 2007.
8. Bazzurro P, Cornell AC. Disaggregation of seismic hazard. *Bulletin of the Seismological Society of America* 1999; **89**(2):501–520.
9. Baker JW, Cornell CA. A vector-valued ground motion intensity measure consisting of spectral acceleration and epsilon. *Earthquake Engineering and Structural Dynamics* 2005; **34**(10):1193–1217.
10. OpenSees. *Open System for Earthquake Engineering Simulation*. Pacific Earthquake Engineering Research Center, University of California: Berkeley, CA. http://opensees.berkeley.edu/ (last accessed January 2007), 2007.
11. Miranda E. Personal communication regarding damping in buildings, 2005.
12. Saatcioglu M, Grira M. Confinement of reinforced concrete columns with welded reinforcement grids. *ACI Structural Journal* 1999; **96**(1):29–39.
13. Haselton CB. Assessing seismic collapse safety of modern reinforced concrete frame buildings. *Ph.D. Dissertation*, Department of Civil and Environmental Engineering, Stanford University, Palo Alto, CA, 2006.
14. Ibarra LF, Medina RA, Krawinkler H. Hysteretic models that incorporate strength and stiffness deterioration. *Earthquake Engineering and Structural Dynamics* 2005; **34**:1489–1511.
15. Ibarra L. Global collapse of frame structures under seismic excitations. *Ph.D. Dissertation*, Department of Civil and Environmental Engineering, Stanford University, Palo Alto, CA, 2003.
16. Fardis MN, Biskinis DE. Deformation capacity of RC members, as controlled by flexure or shear. *Otani Symposium*, Tokyo, Japan, 8–9 September 2003; 511–530.
17. Panagiotakos TB, Fardis MN. Deformations of reinforced concrete at yielding and ultimate. *ACI Structural Journal* 2001; **98**(2):135–147.
18. PEER. *Pacific Earthquake Engineering Research Center*: *Structural Performance Database*. University of California: Berkeley, CA, 2005. Available at http://nisee.berkeley.edu/spd/ and http://maximus.ce.washington.edu/~peera1/ (last accessed January 2007), 2007.
19. ASCE. *ASCE-7-02*: *Minimum Design Loads for Buildings and Other Structures*. American Society of Civil Engineers: Reston, VA, 2002.
20. ATC-40. Seismic evaluation and retrofit of concrete buildings. *Report No. SSC 96-01*, Seismic Safety Commission, Applied Technology Council Project 40, Redwood City, CA, 1996.
21. Vamvatsikos D, Cornell CA. Incremental dynamic analysis. *Earthquake Engineering and Structural Dynamics* 2002; **31**(3):491–514.
22. Zareian F. Simplified performance-based earthquake engineering. *Ph.D. Dissertation*, Department of Civil and Environmental Engineering, Stanford University, Palo Alto, CA, 2006.



DOI: 10.1002/eqe

23. Haselton CB, Baker JW. Ground motion intensity measures for collapse capacity prediction: choice of optimal spectral period and effect of spectral shape. *Eighth National Conference on Earthquake Engineering*, San Francisco, CA, 18–22 April 2006.
24. Goulet C, Haselton C, Mitrani-Reiser J, Stewart JP, Taciroglu E, Deierlein G. Evaluation of the seismic performance of a code-conforming reinforced-concrete frame building—Part I: Ground motion selection and structural collapse simulation. *Proceedings of the Eighth U.S. National Conference on Earthquake Engineering*, San Francisco, CA, 2006.
25. Baker JW, Cornell CA. Uncertainty specification and propagation for loss estimation using FOSM methods. *Proceedings of the Ninth International Conference on Applications of Statistics and Probability in Civil Engineering* (*ICASP9*), San Francisco, CA, 2003.
26. Mitrani-Reiser J, Haselton C, Goulet C, Porter K, Beck J, Deierlein G. Evaluation of the seismic performance of a code-conforming reinforced-concrete frame building—Part II: Loss estimation. *Proceedings of the Eighth U.S. National Conference on Earthquake Engineering*, San Francisco, CA, 2006.
27. Porter KA. Assembly-based vulnerability of buildings and its uses in seismic performance evaluation and risk-management decision-making. *Ph.D. Dissertation*, Stanford University, Stanford, CA. ProQuest Co.: Ann Arbor, MI, 2000.
28. Aslani H, Miranda E. Component-level and system-level sensitivity study for earthquake loss estimation. *Proceedings of the Thirteenth World Conference on Earthquake Engineering*, Vancouver, BC, Canada, 2004.
29. Porter KA, Beck JL, Shaikhutdinov RV. Sensitivity of building loss estimates to major uncertain variables. *Earthquake Spectra* 2002; **18**(4):719–743.
30. RSMeans Corp. *Means Construction Cost Data*. RS Means Co.: Kingston, MA, 2001.
31. Porter KA, Beck JL, Shaikhutdinov RV, Au SK, Mizukoshi K, Miyamura M, Ishida H, Moroi T, Tsukada Y, Masuda M. Effect of seismic risk on lifetime property value. *Earthquake Spectra* 2004; **20**(4):1211–1237.
32. FHWA. Motor vehicle accident costs. *Technical Advisory #7570.2*. Federal Highway Administration U.S. Department of Transportation, Washington, DC, 1994.
33. Shoaf K, Seligson H, Ramirez M, Kano M. Fatality model for non-ductile concrete frame structures developed from Golcuk Population Survey data. *PEER Report 2006*, University of California, Berkeley, CA, 2003.
34. FEMA. *FEMA 222*: *NEHRP Recommended Provisions for the Development of Regulations for New Buildings and NEHRP Maps*, *Part 1*, *1991 Edition*. Federal Emergency Management Agency: Washington, DC, 1992.
35. FEMA. *FEMA 223*: *NEHRP Recommended Provisions for the Development of Regulations for New Buildings*, *Part 2*, *Commentary*, *1991*. Federal Emergency Management Agency: Washington, DC, 1992.



DOI: 10.1002/eqe